Limnol. Oceanogr., 51(1), 2006, 218–228

Prediction of velocity profiles and longitudinal dispersion in emergent salt marsh vegetation

Anne F. Lightbody[1] *and Heidi M. Nepf*
Ralph M. Parsons Laboratory, Department of Civil and Environmental Engineering, Massachusetts Institute of Technology, Cambridge, Massachusetts 02139

Abstract

To predict the behavior of solutes and suspended particles in wetlands, it is necessary to estimate advection and longitudinal dispersion. To better understand these processes, measurements were taken of stem frontal area, velocity, vertical diffusion, and longitudinal dispersion in a *Spartina alterniflora* salt marsh in the Plum Island Estuary in Rowley, Massachusetts. Vegetation volumetric frontal area peaked at 0.067 ± 0.007 cm^{-1} near 10 cm from the bed. If the velocity profile in a dense emergent marsh canopy depends on the local balance between pressure forcing and vegetation drag, the velocity will vary inversely with canopy drag (i.e., velocity is minimum where the frontal area is maximum). In fact, the minimum velocity was observed at 10 cm from the bed. The momentum balance therefore provides a way to predict the velocity profile structure from canopy morphology. The vertical diffusion coefficient also depends on canopy characteristics, such that the vertical diffusion coefficient normalized by the velocity and stem diameter had a constant value of 0.17 ± 0.08 at this study site. The canopy morphology also controls the longitudinal dispersion, observed in this study to be 4 to 27 cm^2 s^{-1}. However, theoretical considerations show that dispersion coefficients of at least 540 cm^2 s^{-1} can occur under typical marsh conditions. Comparisons to other canopies indicate that the prediction of the velocity profile and shear dispersion from canopy morphology can be extended to other emergent canopies and that shear dispersion may vary widely between stands with different physical characteristics.

Fresh- and saltwater wetlands provide habitat for a wide range of plant and animal species, improve water quality, and reduce erosion (Mitsch and Gosselink 1986; Brampton 1992). Understanding the function of these ecosystems requires an understanding of the transport of solutes and particles through these systems, which involves both advection (i.e., the bulk motion associated with the mean flow) and dispersion (i.e., the rate of spreading associated with spatial and temporal deviations from the mean flow). For example, many aquatic organisms rely on the advection and dispersion of chemical signals for information on foraging and mating (e.g., Finelli 2000). Other aquatic organisms rely on advection and dispersion by water currents for the transport and dispersal of nonmotile pollen and gametes (Ackerman 2002), seeds (Middleton 2000), larval stages (Fonseca and Hart 1996), and colonizers (Peterson 1996).

The vertical distribution of longitudinal velocity within vegetated canopies also has important ecological effects. Near-bed velocity affects the flux of solutes between the water column and permeable sediments and the ability of benthic organisms to process particulate material in the flow (Koch and Huettel 2000; Finelli et al. 2002). By reducing near-bed velocity, the presence of vegetation reduces bed stress and thus diminishes resuspension and promotes particle retention within the canopy (López and García 1998; Neumeier and Ciavola 2004). In addition, flow velocity determines the thickness of the laminar sublayer, which controls the transport of nutrients and gases to individual leaves, thereby affecting photosynthetic rates (Koch 1994).

Although several studies have measured the vertical velocity profile within emergent field canopies (e.g., Leonard and Luther 1995; Leonard and Reed 2002; Neumeier and Ciavola 2004), to date no analytic method has been suggested to predict the velocity profile. In addition, the magnitude of dispersion within vegetated canopies is still poorly understood (Arega and Sanders 2004). In this article, we present and test a simple method for estimating the velocity profile and longitudinal dispersion in emergent salt-marsh canopies from knowledge of stem shape and the distribution of vegetation biomass.

Analytic development

We model emergent aquatic vegetation as an array of rigid circular stems of diameter d. The frontal area of vegetation per unit volume is a (units of L^{-1}). In most canopies, both a and d are functions of distance above the bed. The nondimensional quantity ad is a measure of the volume fraction occupied by stems. The x-coordinate is aligned with the direction of mean flow, the y-coordinate is oriented laterally, and the z-coordinate is vertical with $z = 0$ at the bed (Fig. 1A). The longitudinal flow velocity is u, which is spatially averaged over a horizontal scale large enough to eliminate stem-scale heterogeneity. The water depth is represented by h, and the surface slope driving the flow is $\partial\eta/\partial x$. Previous work has used numerical turbulence-closure methods to

[1] Corresponding author (lightbod@mit.edu).

Acknowledgments

We thank Amanda Sorenson, Priyanka Sundareshan, and Nan Yang for their assistance in data collection and analysis, and two anonymous reviewers for their comments. A.F.L. was supported by a National Defense Science and Engineering Graduate Fellowship. The equipment and H.M.N. were supported by the National Science Foundation under grant EAR 0309188. Any opinions, findings, or recommendations expressed in this material are those of the authors and do not necessarily reflect the views of the National Science Foundation.

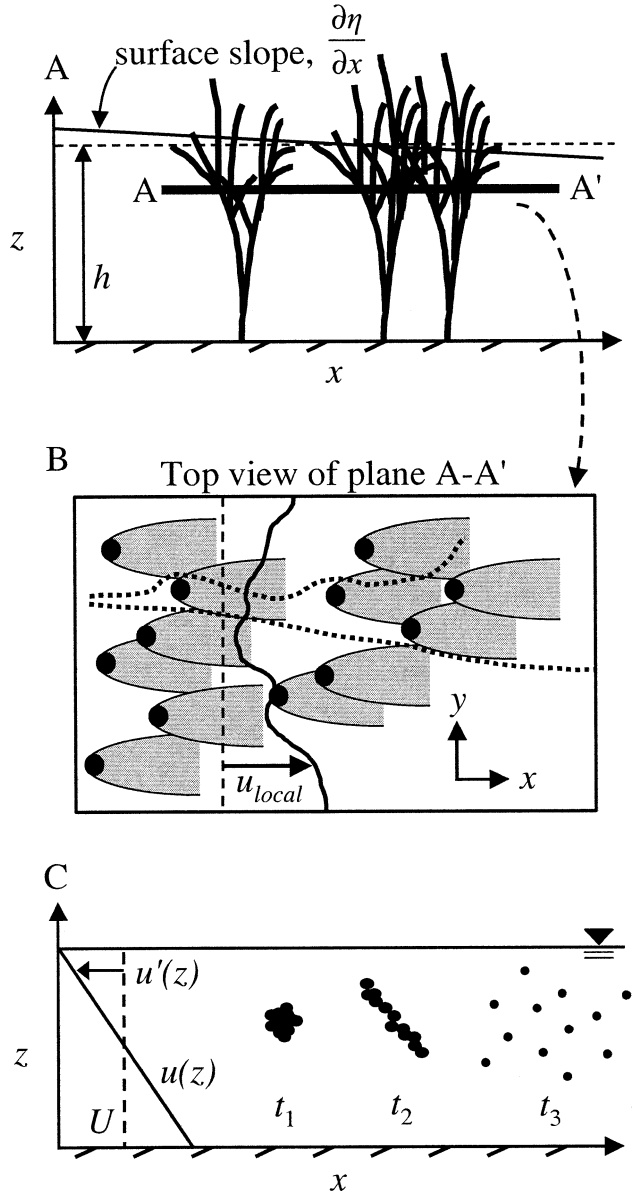

Fig. 1. (A) Definition sketch for an emergent aquatic canopy. The *x*-coordinate is aligned with the horizontal flow direction. (B) A horizontal slice A-A′ shows the local velocity $u_{local}(x, y, z)$, which varies depending on the position of upstream stems. Dashed lines show sample paths of two particles in the flow. (C) Averaging horizontally across slice A-A′ produces the mean longitudinal velocity *u*, which may be a function of height above the bed *z*, producing depth-shear dispersion. A cloud of black particles released at time t_1 experiences the shear as it spreads vertically, producing a net increase in cloud length by time t_3.

solve the full momentum equations in vegetated canopies (Neary 2003), but here we present a simple scaling argument that is useful in field settings. When emergent vegetation is sufficiently dense, the vegetation drag is greater than that attributable to viscous or turbulent stress throughout most of the water column, and the influence of the bed is limited to a region within approximately one stem diameter *d* of the bed (Nepf et al. 1997). Additionally, assuming steady, uniform, fully developed flow and hydrostatic pressure, the momentum equation reduces to a simple balance between the vegetation drag and pressure forcing terms. Scaling analysis confirms that this model is reasonable given typical conditions in a salt marsh system (Burke and Stolzenbach 1983). Adopting a quadratic expression for the drag force on the plant stems, the momentum equation becomes:

$$\frac{1}{2}C_d a u^2 = g\frac{\partial \eta}{\partial x} \tag{1}$$

where *g* is the gravitational acceleration. The vegetation drag coefficient C_d is a function of the stem Reynolds number $\mathrm{Re}_d = ud/\nu$, where ν is the kinematic viscosity of water. C_d may also be a function of stem shape. The drag coefficient for a circular cylindrical stem within a canopy may be represented by that for an isolated circular cylinder (e.g., White 1991, p. 183) when the canopy density $ad < 0.1$ (Nepf 1999; Stone and Shen 2002). Noncircular stems can be accommodated in Eq. 1 if the drag coefficient can be estimated.

Previous work has shown that the depth-averaged form of Eq. 1 correctly predicts the depth-averaged velocity within an emergent canopy (Peterson et al. 2004); we consider the vertical variation in vegetation density in order to resolve the vertical structure in the velocity profile. Because $\partial\eta/\partial x$ is not a function of vertical position in the water column, the quantity $C_d a u^2$ is constant over depth. The velocity profile therefore varies inversely with canopy morphology; specifically, $u(z) \propto 1/\sqrt{C_d(z)a(z)}$. From this it follows that normalized velocity profiles should have a single common shape that depends only on canopy morphology. Let $\tilde{u}$ represent the velocity at a reference height above the bed where vegetation drag dominates, and let $\tilde{a}$ represent the frontal area density and $\tilde{C}_d$ the drag coefficient at this same height. Then, velocity profiles normalized by $\tilde{u}$ should follow a single profile shape that depends only on the profile $C_d(z)a(z)$:

$$\frac{u(z)}{\tilde{u}} = \sqrt{\frac{\tilde{C}_d \tilde{a}}{C_d(z)a(z)}} \tag{2}$$

Because C_d is related through the Reynolds number to the flow velocity, Eq. 2 can only be solved iteratively for the vertical shape of the velocity profile $u(z)/\tilde{u}$, and the profile shape may change slightly depending on the magnitude of $\tilde{u}$. However, for rigid vegetation with $ad < 0.10$ and $10 < \mathrm{Re}_d < 10{,}000$, it has been suggested that C_d is not a strong function of stem density or Reynolds number (Koch and Ladd 1997; Nepf 1999; Stone and Shen 2002). For these conditions, we may assume that the drag coefficient C_d is approximately constant over depth, and Eq. 2 reduces to

$$\frac{u(z)}{\tilde{u}} = \sqrt{\frac{\tilde{a}}{a(z)}} \tag{3}$$

Note that Eqs. 2 and 3 will not hold for submerged vegetation, as turbulent stress cannot be neglected in those conditions.

The longitudinal dispersion constant K_x describes the rate of growth of spatial variance σ_x^2 of a cloud of solute or particles:

$$K_x = \frac{1}{2}\frac{d\sigma_x^2}{dt} \tag{4}$$

where t is the time since release. Dispersion arises from spatial heterogeneity in the velocity field. Within a marsh canopy, there are several scales of velocity heterogeneity. First, Fig. 1B shows that velocity heterogeneity exists at the stem scale because of the velocity depressions directly downstream of each stem. The stem-scale velocity heterogeneity, described by $u_{\text{local}}(x, y, z)$, can produce dispersion as follows. When a particle cloud passes through the vegetation, particles passing through more stem wakes will travel more slowly than particles that travel through fewer stem wakes, causing the distribution of particles to stretch out longitudinally. This mechanical dispersive process is represented by the stem-shear dispersion coefficient K_d, where the subscript indicates dispersion resulting from velocity heterogeneity on the scale of the stem diameter. When every particle has sampled a sufficient number of wakes, this process reaches a Fickian limit, and K_d achieves a constant value.

The velocity u appearing in Eqs. 2 and 3 represents a horizontal average over a scale much larger than d. This average removes the stem-scale heterogeneity. However, following from Eqs. 2 and 3, u may vary over depth if a varies over depth. This depth-scale heterogeneity produces depth-shear dispersion (Fig. 1C), described by the coefficient K_h. Once a cloud of material has spread over depth, so that the vertical heterogeneity in velocity has been fully sampled, the Fickian limit is reached, and K_h will be a constant. Before the cloud spreads over depth, K_h increases with time as the cloud grows. Below, we develop expressions for K_h before and after the Fickian limit is reached.

Finally, vegetation morphology or density may also vary across the horizontal plane over a length-scale $L_a = O(10–100$ m) (Christiansen et al. 2000; Proffitt et al. 2003). When clouds grow to this scale, the horizontal heterogeneity contributes another mechanism of dispersion similar to the macrodispersion observed in groundwater flow through an array of lenses of varying conductivity (e.g., Cherblanc et al. 2003; Russo 2003). The dispersion coefficient usually increases with the scale of the velocity heterogeneity (Nepf 2004). Thus, as a cloud grows to sample larger scales of heterogeneity, the rate of dispersion increases. In most wetland applications, however, the macroscale $> O(100$ m) is modeled explicitly (e.g., Thompson et al. 2004), so it is not necessary to define a dispersion constant at this scale. In addition, at this scale, branching channel networks, a common feature of coastal wetlands, become important agents of dispersion (Rinaldo et al. 1991; Smith and Daish 1991).

This study focuses on the dispersion processes arising from stem-scale and depth-scale velocity heterogeneity, which are important within regions of vegetation characterized by a single morphology [$a \neq f(x, y)$]. Within such regions, depth-scale and stem-scale dispersion processes contribute additively to and dominate the total dispersion K_x:

$$K_x = K_d + K_h \tag{5}$$

In the Fickian limit the stem-scale dispersion may be approximated as

$$K_d = \frac{1}{2}C_d^{3/2}ud \tag{6}$$

for volumetric density $ad < 0.1$ (White and Nepf 2003). Equation 6 is valid at time $t >> (au)^{-1}$ after the initial release (White and Nepf 2003), or at distances $x >> a^{-1} \approx 10$ cm for a typical marsh canopy. Because our observations of dispersion are made over distances much greater than 10 cm, we do not here consider the pre-Fickian behavior of K_d.

Next consider the depth-scale shear dispersion. In the Fickian limit ($t > t_{\text{Fickian}} = 0.4\,h^2/D_z$, where D_z is the vertical diffusion), K_h is given by Taylor's analysis (e.g., Fischer et al. 1979, p. 91):

$$K_h = -\frac{1}{h}\int_0^h u' \int_0^z \frac{1}{D_z}\int_0^z u'\, dz\, dz\, dz \tag{7}$$

where $u'(z) = u(z) - U$ is the deviation from the depth-averaged velocity U. To first order, turbulent vertical diffusion is related to the flow speed u and stem morphology (Nepf 1999):

$$D_z = \alpha\sqrt[3]{C_d a d}\, ud \tag{8}$$

From laboratory data, the proportionality constant $\alpha = 0.1–0.2$; mechanical dispersion may augment this constant for denser canopies ($ad > 0.10$; Nepf 2004). Note that $(\sqrt[3]{ad})$ is relatively insensitive to changes in volume fraction ad. For example, if ad doubles, $(\sqrt[3]{ad})$ will only increase by 25%. Thus, even for moderate variation in ad over depth, D_z/ud is approximately constant over depth.

Assuming that Eq. 2 holds over the full water depth, depth-shear dispersion can be predicted from canopy characteristics. Normalizing D_z by ud and u' and u by U, Eq. 7 can be rewritten as

$$K_h = -\frac{U}{hd}\int_0^h \frac{u'}{U}\int_0^z \left(\frac{U}{u}\right)\left(\frac{ud}{D_z}\right)\int_0^z \frac{u'}{U}\, dz\, dz\, dz \tag{9}$$

Let $\Im$ represent the nondimensional velocity shape factor

$$\Im = -\frac{1}{h^2 d}\int_0^h \frac{u'}{U}\int_0^z \frac{U}{u}\int_0^z \frac{u'}{U}\, dz\, dz\, dz \tag{10}$$

Using Eq. 2, $\Im$ is shown to be a function solely of canopy morphology:

$$\Im = -\frac{1}{h^2 d}\int_0^h \left(\sqrt{\frac{\overline{C_d a}}{C_d a}} - 1\right)\int_0^z \sqrt{\frac{C_d a}{\overline{C_d a}}} \times \int_0^z \left(\sqrt{\frac{\overline{C_d a}}{C_d a}} - 1\right) dz\, dz\, dz \tag{11}$$

where the overbar on $\overline{C_d a}$ indicates the value of $C_d a$ corresponding to the depth-averaged velocity U, specifically

$$\overline{C_d a} = \left[\frac{1}{h}\int_0^h (C_d a)^{-1/2}\, dz\right]^{-2}$$

When D_z/ud is approximated as a constant, the normalized depth-shear dispersion coefficient K_h/Uh is given by

$$\frac{K_h}{Uh} = \left(\frac{ud}{D_z}\right)\Im \tag{12}$$

which can be written as a function of only C_d, a, d, and h using Eqs. 8 and 11.

Before the cloud mixes over depth, K_h and, thus, K_x are not constant. However, we can estimate the evolution at early times by assuming that the local velocity profile is approximately linear (e.g., Neumeier and Ciavola 2004). Then we can adapt the analytic solution of Mauri and Haber (1986) for dispersion in linear shear; i.e., for material released at height z_r above the bed, the variance will evolve as

$$\sigma_x^2 = \frac{2}{3}u_r^2 D_z \left[\left(\frac{\partial}{\partial z}\frac{u}{u_r}\right)\bigg|_{z_r}\right]^2 t^3 + \qquad 2K_d t \tag{13}$$

depth-scale shear stem-scale shear

where u_r is the velocity at the release height and

$$\left(\frac{\partial}{\partial z}\frac{u}{u_r}\right)\bigg|_{z_r}$$

is the slope of the normalized velocity profile at the release height. The first term in Eq. 13 represents the contribution of K_h and is non-Fickian; specifically, its contribution increases as t^3. This reflects the fact that as the cloud grows vertically with time, it samples more velocity heterogeneity and so spreads more rapidly. The second term represents the contribution of K_d, which we assume has reached Fickian behavior. The contribution of turbulent longitudinal diffusion is not considered, as it is small compared to K_d. Using Eqs. 2 and 6, the evolution of variance in the near field (Eq. 13) can be written thus:

$$\sigma_x^2 = \frac{2}{3}u_r^3 d\left(\frac{D_z}{u_r d}\right)\left[\left(\frac{\partial}{\partial z}\sqrt{\frac{C_{d,r}a_r}{C_d a}}\right)\bigg|_{z_r}\right]^2 t^3 + \qquad u_r d C_d^{3/2} t \tag{14}$$

depth-scale shear stem-scale shear

Substituting this expression into Eq. 4 and differentiating shows that the nondimensional longitudinal dispersion before the cloud has mixed over depth is a function of canopy morphology (C_d, a, and d) and increases with the distance from the source x:

$$\frac{K_x}{u_r d} = \left(\frac{D_z}{u_r d}\right)\left[\left(\frac{\partial}{\partial z}\sqrt{\frac{C_{d,r}a_r}{C_d a}}\right)\bigg|_{z_r}\right]^2 x^2 + \qquad C_d^{3/2} \tag{15}$$

depth-scale shear stem-scale shear

Therefore, because $D_z/u_r d$ is a function of ad (Eq. 8), K_x can be predicted from information about canopy morphology, even at early times before the Fickian limit is reached.

Materials and methods

Field measurements of stem frontal area, flow velocity, vertical diffusion, and small-scale longitudinal dispersion were carried out at the Plum Island Estuary in Rowley, Massachusetts, in July and August of 2003. The study site (42.727°N, 70.848°W) was a monoculture of the tall form of *S. alterniflora* on a bar in the middle of the Rowley River (Fig. 2); the local tidal range is approximately 1.5 m, and velocities in the nearby river channel reach 2–4 m s^{-1}. *S. alterniflora* is the dominant plant species in salt marshes in the eastern United States; the tall form can reach 2–3 m in height and has smooth, relatively rigid leaves and culms that are 5–15 mm in diameter (Valiela et al. 1978; Silberhorn 1982, p. 101). No measurements were taken when the vegetation was fully submerged or when waves from wind or boats were larger than 5 cm. All velocity measurements, dye releases, and dye measurements occurred at least 2 m from the edge of the vegetation. Previous studies have shown that vertical velocity profiles within the canopy are established within 50 cm of the edge of a vegetated bed when $ad > 0.003$ (Gambi et al. 1990), a condition that is met here.

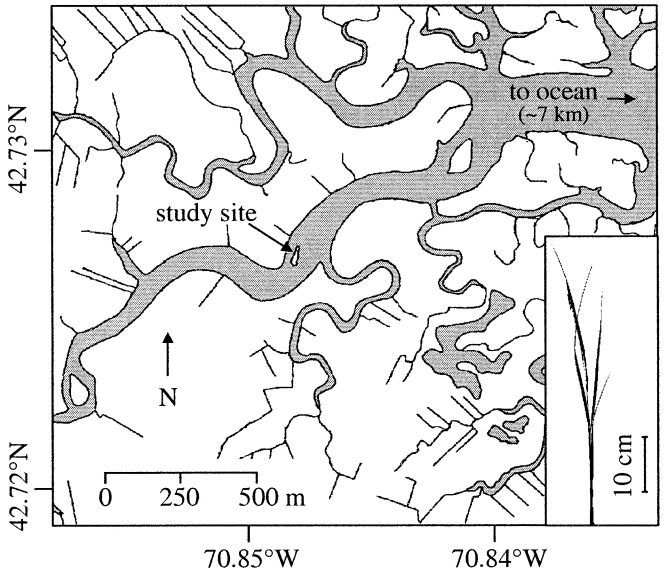

Fig. 2. Map showing the field site located on an island in the middle of the Rowley River, Plum Island Estuary, Rowley, Massachusetts. Open water is shown in gray. Inset shows a representative *S. alterniflora* stem from the field site.

Four times during the study period, all of the stems inside a 0.11-m^2 quadrat were harvested and immediately photographed in front of a white background using a 4.1-megapixel digital camera (DSC-S85 Cyber-shot, Sony). The number of pixels within each stem was counted, the frontal area of each stem was determined through a pixel conversion scale that corrected for parallax, and the volumetric frontal area a was then calculated by summing over all stems within the quadrat. There were two major sources of uncertainty in the image processing. First, a comparison of photographs of different views of a subset of 55 stems revealed that the orientation of the stem during photography contributed an uncertainty of 20% to the estimated value of a. Second, the appropriate value of the threshold used to separate the stem from the background was selected by hand for each image, and a difference of 1% in the threshold value changed the final calculated area by approximately 5%. Stem diameter measurements were performed on stems collected on 28 October 2002. Calipers were used to measure the width of each leaf and stem at 10 cm and 20 cm above the bed on a total of 33 plants collected from the field site.

Water velocity through the canopy was measured using a two-dimensional, sideways-looking field acoustic Doppler

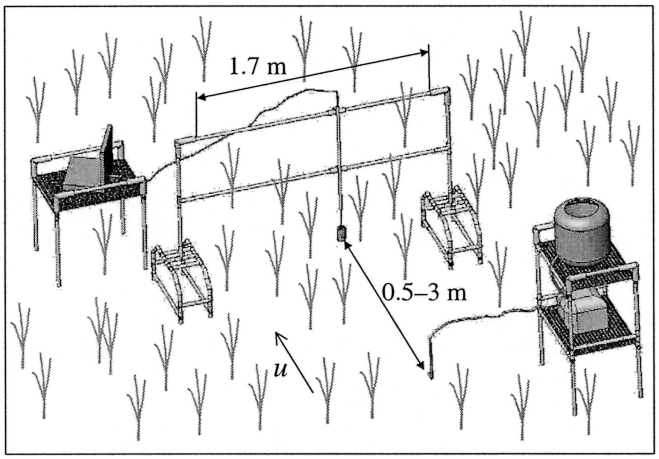

Fig. 3. Set-up for dye releases. Dye was injected at various distances upstream of the fluorometer, which was located on a traverse allowing lateral and vertical adjustment.

velocimetry probe (FlowTracker, SonTek/YSI). The probe was mounted on a gauging staff and used to take 2- to 5-min records at 1 Hz at 5-cm intervals above the bed. Before starting each profile, we anchored a piece of plastic mesh with the same footprint as the probe head to the bed below the probe to guide plants away from the measurement volume. Because flow direction was changeable, horizontal flow speed was calculated as the absolute value of the vector sum of the horizontal velocity components.

To correct for small changes in mean velocity over the course of a profile measurement, each velocity profile began and ended with a measurement at the same height above the bed. This height was high in the water column, where velocities were highest. Each measurement during the profile was then scaled to what it would have been if it had been taken at the beginning of the measurement period using linear interpolation from the repeated measurements. Individual profiles were selected for further analysis using the following three criteria: they consisted of measurements at three or more different distances from the bed, they had a monotonic velocity increase above 15 cm from the bed, and the mean flow direction changed by less than 60° over the entire vertical profile.

Vertical diffusion was measured by fitting theoretical profiles (*see* following) to measured vertical concentration profiles downstream of a continuous dye release (Fig. 3). Rhodamine WT was pumped using a field sampling pump (Masterflex Environmental Sampler, Cole-Parmer) through 0.64-cm–diameter tubing to a needle placed horizontally in the flow between 9 and 12 cm from the bed. The needle was placed so that it was not immediately upstream of any stems. The outlet velocity of the dye was carefully matched to the velocity of the ambient flow, which was estimated by timing a slug of dye traveling a known distance. The slug-release method of velocity measurement has been shown to correlate well with direct measurements of mean velocity (Hosokawa and Horie 1992). Dye concentration was measured 0.5 m to 3 m downstream using an in situ fluorometer (Seapoint Sensors), which was attached to an OS200 conductivity–temperature–depth profiler (Ocean Sensors). The sampling frequency of the fluorometer was 8 Hz.

The dye meandered laterally in the field over a timescale of several minutes in response to large-scale turbulence and to changes in flow pattern over the tidal cycle. As a result, the fluorometer was used to take repeated lateral transects, each lasting less than 20 s, through the dye cloud and perpendicular to its course at a known longitudinal position x. Because the transect time was much shorter than the meander timescale, each transect that reached a baseline concentration at each end was assumed to capture the true maximum concentration in the plume. The maximum concentrations measured on the transect were then averaged to define a single maximum concentration at each height above the bed, which was presumed to represent the plume centerline. For a continuous release in a constant velocity field, the dye concentration along the lateral centerline can be written (Fischer et al. 1979, p. 49)

$$C(x, z) = \frac{\dot{m}u_r}{4\pi x\sqrt{D_y D_z}}\exp\left[-\frac{u_r(z - z_r)^2}{4D_z x}\right] \qquad (16)$$

where $\dot{m}$ is the dye injection rate and D_y is the lateral diffusion constant. The measured variation in maximum concentration over depth was fit to the exponential term in Eq. 16 in a least-squares sense, with D_z as one of the fitting parameters. The error in the value of D_z was calculated by determining what change in D_z yielded a 5% change in the sum of least squares.

Longitudinal dispersion was calculated from individual slug releases of dye. A syringe was used to release Rhodamine WT at mid-depth from 0.64-cm–diameter tubing, with the end oriented parallel to the direction of flow. Releases took 0.5–2 s each, which was much less than the travel time to the fluorometer (31–691 s), so the releases were assumed to be instantaneous. The fluorometer was positioned at mid-depth and directly downstream of the release point. Slugs of dye were released at z_r = 15–44 cm above the bed and for local flow speeds of u_r = 0.2–5.4 cm s^{-1}.

Between 10 and 30 releases at mid-depth were performed for each of nine different distances between the release point and the fluorometer. Concentration profiles were first normalized by the total area under the curve, which makes the shape of the profile independent of the initial mass, lateral and vertical diffusion, and the lateral position of the cloud center (White and Nepf 2003). Next, the time record of concentration was used to calculate the second temporal moment σ_t^2. It was assumed that each cloud did not change appreciably as it passed the fluorometer, so the temporal moment could be translated into a spatial moment σ_x^2 by multiplying by its average travel speed: i.e., $\sigma_x^2 = u_r^2\sigma_t^2$. To tease apart the effects of velocity and vertical position (related to vegetation density), the slug release data were binned into three different vertical ranges (z_r = 15–25 cm, z_r = 25–35 cm, and $z_r > 35$ cm) and four different velocity levels ($u_r < 1.5$ cm s^{-1}, u_r = 1.5–2.5 cm s^{-1}, u_r = 2.5–3.5 cm s^{-1}, and u_r = 3.5–5.5 cm s^{-1}).

For each bin, two comparisons were made between observations and theory. First, the observed evolution of tracer variance was compared to the evolution predicted from Eq.

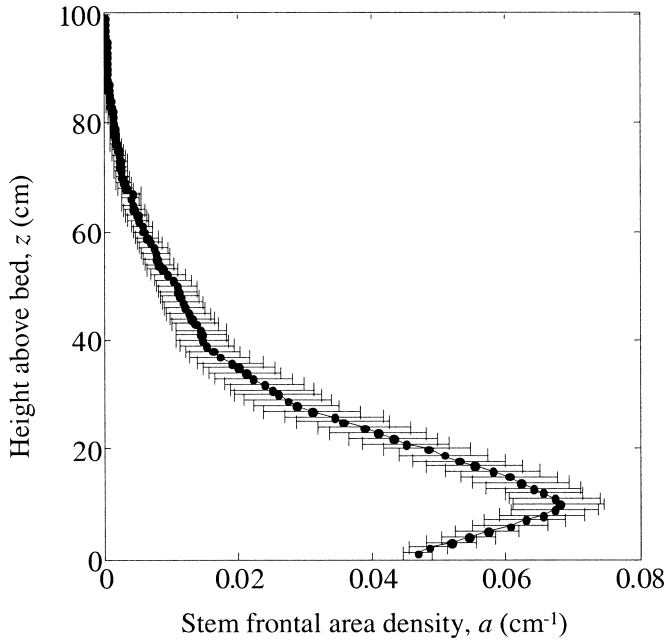

Fig. 4. Average stem frontal area density. The value at each height above the bed is the mean of the total stem frontal area from four quadrats. Horizontal bars indicate standard error of the mean of the different quadrats.

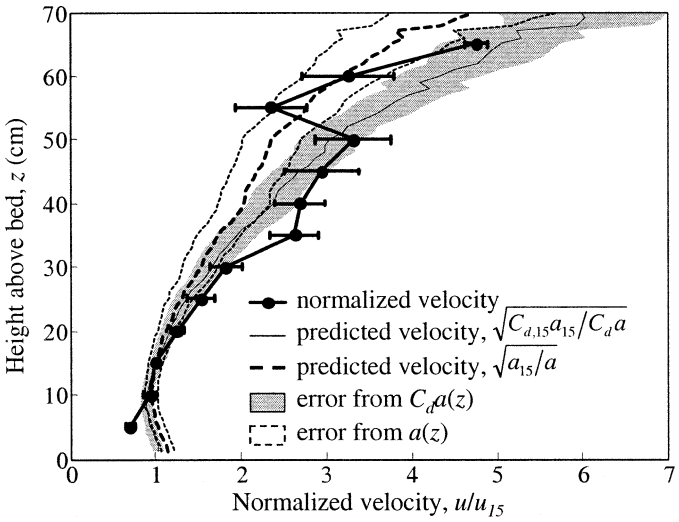

Fig. 5. Vertical profile of horizontal velocity. Each point is the mean of 2 to 45 velocity measurements normalized by the velocity at 15 cm above the bed, u_{15}. Horizontal bars indicate standard error of the mean of the different normalized measurements. Two theoretical velocity curves are also shown, both calculated using data in Fig. 4: $\sqrt{C_{d,15}a_{15}/C_d a}$ (thin solid line, with error in gray), where C_d is calculated separately for each height above the bed in each profile, and $\sqrt{a_{15}/a}$ (thick dashed line, with error outlined by thin dashed lines), where C_d is assumed to be constant over depth.

14. Second, an observed dispersion coefficient was estimated by fitting the form of Eq. 13 to the observed evolution of variance, specifically

$$\sigma_x^2 = Pt^3 + 2K_d t \tag{17}$$

with K_d estimated from Eq. 6 and P the only fitting parameter. Plugging Eq. 17 into Eq. 4 provides the observed total dispersion $K_{x,obs}$ at a specified distance x_{pred} from the release:

$$K_{x,obs} = \frac{3}{2}\left(\frac{x_{pred}}{u_r}\right)^2 P + K_d \tag{18}$$

Results

Stem diameter d was found to be 0.17 ± 0.08 cm (mean ± standard error of the mean; n = 33 stems) at 10 cm above the bed and 0.12 ± 0.06 cm at 20 cm above the bed. We will here assume an average stem diameter of 0.15 ± 0.07 cm throughout the canopy. This value is comparable to those measured elsewhere; for example, Valiela et al. (1978) reported a median stem diameter of just less than 0.2 cm for *S. alterniflora* stems.

Figure 4 shows the mean vegetation frontal area density averaged over four different quadrats. Both the shape and the magnitude of the frontal area density curve were constant over the course of the study (data not shown). Note that the frontal area density is a strong function of height above the bed, peaking at a value of a = 0.067 ± 0.007 cm^{-1} (ad = 0.010 ± 0.005) at 11 cm from the bed and then slowly diminishing, reaching a = 0.011 ± 0.003 cm^{-1} (ad = 0.002 ± 0.001) at 50 cm from the bed and declining to nearly zero at 100 cm above the bed. Leonard and Luther (1995) reported a similar profile in a *S. alterniflora* marsh, with the peak density at 10–15 cm from the bed, where leaves branch off from the stem.

Flow speeds through the marsh canopy varied over the tidal cycle from 0.1 to 24 cm s^{-1}, producing Re_d = 2–360; most measurements were between 2 and 6 cm s^{-1}. Similarly, Leonard and Luther (1995) measured velocities of $1 < u <$ 15 cm s^{-1} through an emergent creek-side stand of *S. alterniflora*, with speeds declining to $0.75 < u < 5$ cm s^{-1} at interior marsh sites.

Next we consider whether the velocity profiles exhibit a characteristic shape when normalized by a reference velocity (Eqs. 2 and 3). All velocity measurements were normalized by the velocity at 15 cm above the bed, $\tilde{u} = u_{15}$, which was selected because it is both farther than one stem diameter from the bed and above the bed microtopography, so bottom boundary roughness has a limited effect (Nepf et al. 1997), and also far enough below the surface that Reynolds stresses due to the wind should be negligible. Linear interpolation was used to find the velocity at z = 15 cm when no measurement was taken at this height. The composite velocity profile shown in Fig. 5 reveals that this normalization makes velocity profiles taken under different flow conditions (u_{15} = 0.7–24 cm s^{-1}, h = 11–82 cm) follow a single profile, confirming Eq. 2. Note that the velocity points above 50 cm are undersampled compared to those lower in the canopy, which may explain the observed kink. The shape of the normalized profile resembles that observed previously in laboratory and field studies of emergent natural vegetation, with the lowest velocity (u_{10}/u_{15} = 0.9 ± 0.1) located where the frontal area density is highest (Burke and Stolzenbach 1983; Leonard

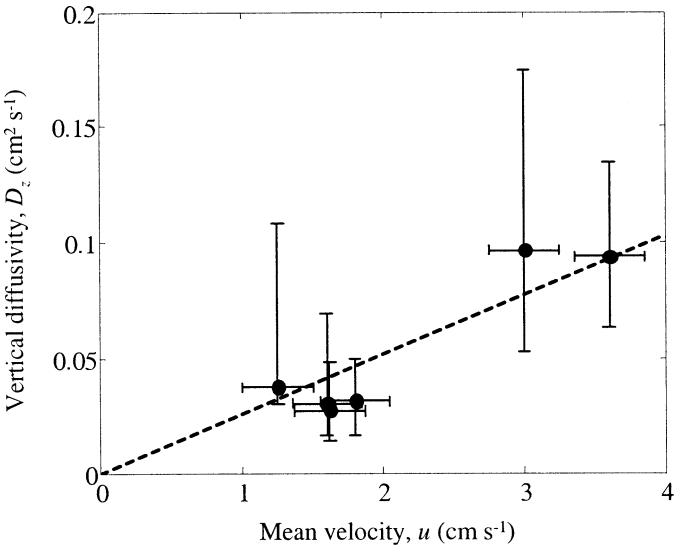

Fig. 6. Vertical diffusivity constants measured at different locations downstream of a continuous dye release. Vertical bars indicate the values of D_z that produce a 5% change in the least-squares residuals for the Gaussian curve fit (Eq. 16). Horizontal bars indicate the standard error of the mean velocity for each diffusivity measurement (i.e., each separate vertical profile). The dashed line is the least-squares linear fit through zero, for which $D_z = (0.026 \pm 0.002)u$, $n = 6$, $p = 0.006$, $r^2 = 0.87$.

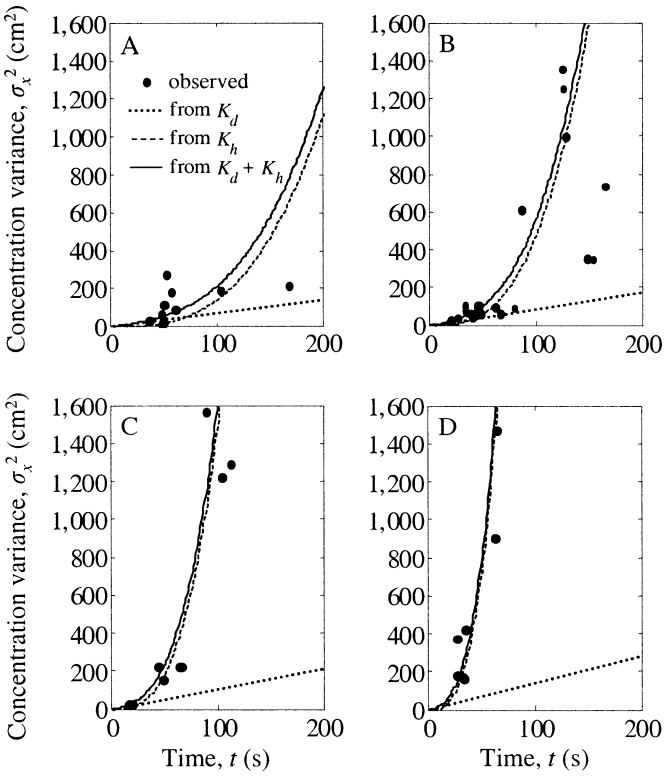

Fig. 7. The spatial variance of evolving slug releases as a function of time is shown for slugs from all four velocity bins released at a height above the bed of $z_r = 26$–33 cm: (A) $u_r < 1.5$ cm s^{-1}, (B) $u_r = 1.5$–2.5 cm s^{-1}, (C) $u_r = 2.5$–3.5 cm s^{-1}, and (D) $u_r = 3.5$–5.5 cm s^{-1}. For each bin, the dotted line is the predicted spatial variance from stem-shear dispersion, K_d (Eq. 6). The dashed line is the predicted spatial variance from depth-shear dispersion, K_h, calculated using the slope of the $\sqrt{C_{d,15}a_{15}/C_d a}$ curve over the region $z = 15$–50 cm (first term in Eq. 15). The solid line is the predicted total spatial variance from the sum of these two sources (Eq. 14). Note that all three lines are not fit but are predicted from information about the vegetation (i.e., from data in Fig. 4).

and Luther 1995; Shi et al. 1995). Now established, the normalization used here can allow the extrapolation of the full velocity profile from just one or two measurements, in analogy to the use of logarithmic profiles over bare beds.

In addition, the normalized velocity profile agrees well with that predicted using Eq. 2 (Fig. 5). Here, the curve of $\sqrt{C_{d,15}a_{15}/C_d a}$ is calculated using a single-cylinder approximation for C_d (White 1991, p. 183) based on the Re_d corresponding to the velocity measured at each height above the bed, and these separate realizations are then averaged. This predicted velocity profile therefore includes $C_d(z)$ in the normalization, which makes calculation difficult for two reasons: first, C_d is not well characterized for an array of stems, and second, C_d is a nonlinear function of Re_d. For comparison, Fig. 5 also shows the predicted velocity profile from Eq. 3, which assumes that C_d is constant over depth. This latter curve also provides a reasonably good fit to observations. For later use in calculating the dispersion constant, in the region $z = 15$–50 cm, the slope of the curve $\sqrt{C_{d,15}a_{15}/C_d a}$ is 0.061 ± 0.001, and the slope of the curve $\sqrt{a_{15}/a}$ is 0.042 ± 0.006.

The predicted velocity profiles deviate most noticeably from the observations within 10 cm of the bed, which is where microtopography may contribute additional drag. In addition, by only considering intact stems, our method of characterizing the frontal area neglected some wrack, which may be an important component of $a(z)$ near the bed (Neumeier and Ciavola 2004). The predicted velocity profile also deviates from the observed profile above 70 cm from the bed. In this region, it is likely that wind shear and other surface processes may be important. For example, Jenter and Duff (1999) attributed higher velocities in the top 15 cm of the water column in a bed of *Cladium jamaicense* to wind-induced shear.

The above vertical diffusion model predicts a positive linear correlation between vertical diffusion and ambient flow speed (Eq. 8). Within error, this model agrees with the field measurements (Fig. 6). Following Eq. 8, turbulent diffusivity is assumed to approach zero at zero velocity, which yields $D_z/ud = 0.17 \pm 0.08$. Here $ad = 0.005$–0.010, which indicates that $\alpha \approx 0.7 \pm 0.4$ in Eq. 8. This value of D_z/ud is slightly higher than but comparable to the range observed by Nepf et al. (1997) in a laboratory flume study of an emergent dowel array ($D_z/ud = 0.04 \pm 0.01$ for $ad = 0.014$ and $D_z/ud = 0.09 \pm 0.01$ for $ad = 0.053$) and the value of $D_z/ud = 0.10$ observed by Saiers et al. (2003) when measuring particle transport in the Everglades through a canopy of *Eleocharis cellulosa* and *Eleocharis elongata* with $ad \approx 0.005$. Taken together, these results indicate that vertical diffusion is tied to stem density, as predicted by theory, but is also higher in the field than in a laboratory array of purely vertical cylinders. The higher vertical diffusion in the field, which approaches the value observed for lateral diffusion in

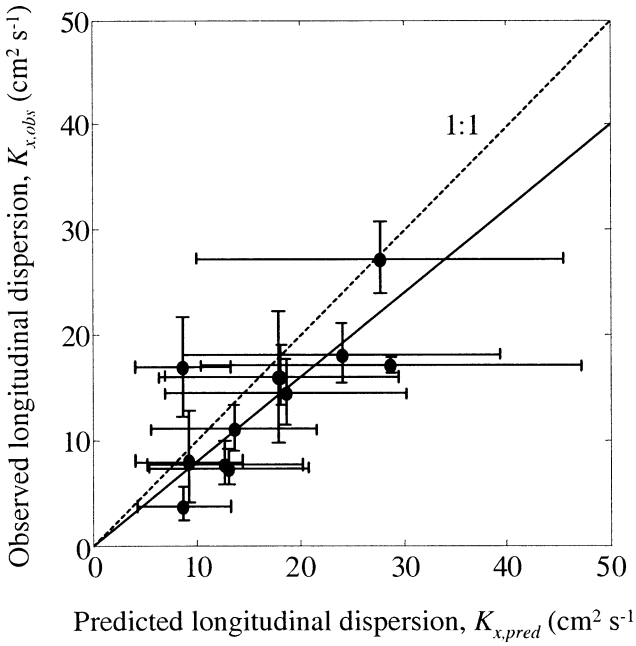

Fig. 8. Comparison between observed and predicted longitudinal dispersion constants for 12 different velocity and depth bins 250 cm downstream of a slug release. Observed longitudinal dispersion constants (Eq. 18, with P fit to data using Eq. 17 and K_d predicted using Eq. 6) are compared to predicted longitudinal dispersion constants (Eq. 15, using the average slope of $\sqrt{C_{d,15}a_{15}/C_d a}$ over z = 15–50 cm, the measured value of D_z/ud, and K_d predicted using Eq. 6). Horizontal bars indicate the uncertainty in the value of $K_{x,pred}$. Vertical bars indicate the values of $K_{x,obs}$ that produce a 5% change in the least-squares residuals for the power-law fit in Eq. 17. The solid line indicates the least-squares linear fit through zero to the data, for which $K_{x,obs} = (0.80 \pm 0.07)\, K_{x,pred}$, $n = 12$, $p = 0.004$, $r^2 = 0.59$; the dashed line indicates a 1 : 1 relationship.

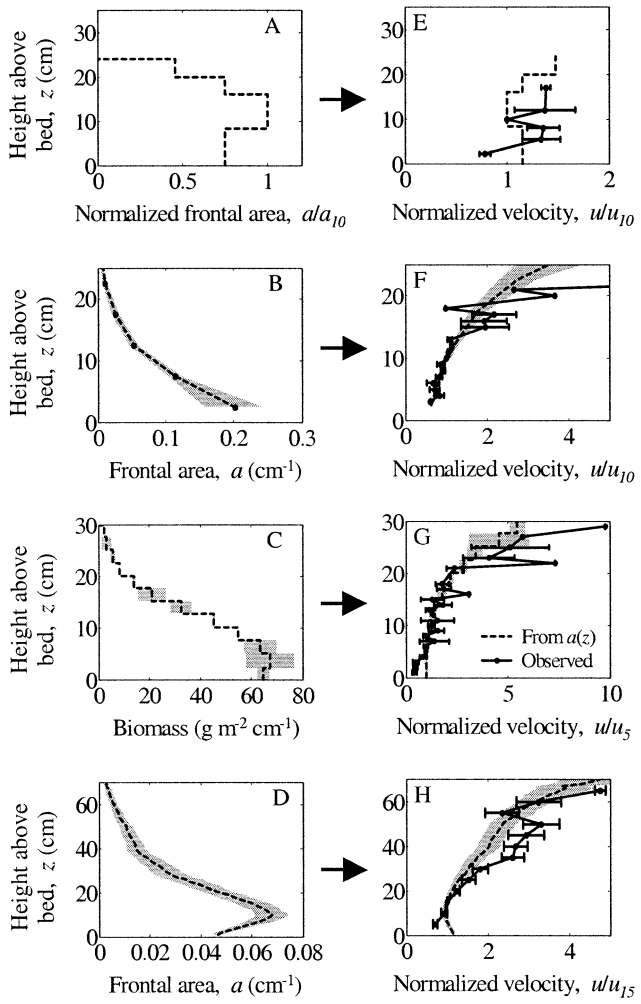

Fig. 9. Comparison of $a(z)$ and $u(z)$ in several different canopies. (A) Normalized frontal area (dashed line, with uncertainty where available in gray) in a *S. alterniflora* canopy (Leonard and Luther 1995); (B) frontal area in a *S. alterniflora* marsh (Burke and Stolzenbach 1983); (C) biomass distribution in a *S. maritima* canopy (Neumeier and Ciavola 2004); and (D) frontal area distribution in the present study. Panels E, F, G, and H, respectively, compare the normalized velocity profiles predicted by these frontal area density curves using Eq. 3 (dashed line, with uncertainty where available in gray) to measured velocity profiles in these canopies (points connected by solid line, with uncertainty indicated by horizontal bars).

a vertical array, likely results from stems and branches with orientations other than vertical, because horizontal components of stems and branches enhance vertical diffusion by producing turbulence with a vertical component (Nepf 2004).

Figure 7 shows the evolution of tracer variance in 4 out of the 12 different release-height and velocity bins. As expected from Eq. 13, the concentration variance increases nonlinearly as a function of time, indicating that these clouds have not reached the Fickian limit. The predicted variance resulting from the sum of stem-shear and depth-shear processes (Eq. 14) is shown in Fig. 7 as solid lines. Note that these curves are not fit to the data but are predicted only from canopy morphology ($a(z)$ and d) and the measured value of D_z/ud, which is assumed constant over depth. Figure 7 also illustrates how the rate of increase in variance increases with velocity, as is predicted by Eq. 14. Also, note that near the point of release, stem-shear dispersion dominates, but depth-shear dispersion dominates farther downstream. This trend is most clearly seen in Fig. 7A, where the two lines cross at approximately 80 s, which corresponds to approximately 80 cm from the point of release for this bin; the other bins also exhibit a transition at approximately 80 cm downstream of the release.

A nonlinear fit was used to estimate an observed dispersion constant from the concentration variance (Eqs. 17 and 18) at x_{pred} = 250 cm. Predicted dispersion coefficients $K_{x,pred}$ were calculated from Eq. 15 using the slope of the $\sqrt{C_{d,15}a_{15}/C_d a}$ and $\sqrt{a_{15}/a}$ curves between 15 and 50 cm from the bed. When the $\sqrt{C_{d,15}a_{15}/C_d a}$ curve is used, $K_{x,obs} = (0.80 \pm 0.07)K_{x,pred}$ ($n = 12$, $p = 0.004$, $r^2 = 0.59$), indicating that the observed dispersion is on the same order of magnitude as the predicted shear dispersion (Fig. 8). If $K_{x,pred}$ is calculated using the slope of $\sqrt{a_{15}/a}$, $K_{x,obs} = (1.6 \pm 0.1)K_{x,pred}$ ($n = 12$, $p = 0.004$, $r^2 = 0.59$). The large observed error bars on the predicted dispersion coefficient are due primarily to uncertainty in d and D_z/ud.

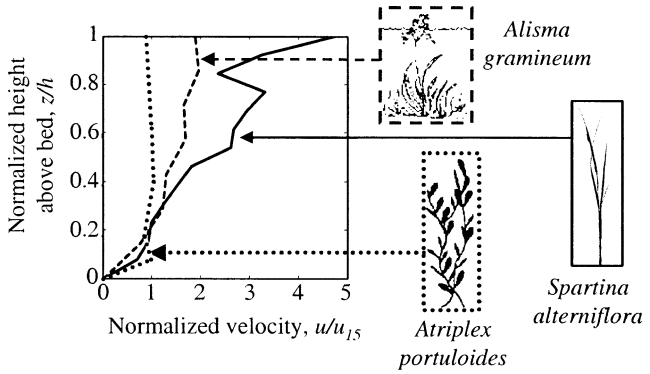

Fig. 10. Velocity profiles measured in three different field canopies, making the assumption that velocity approaches zero at the bed. *Atriplex portuloides* data from Leonard and Reed (2002); *Alisma gramineum* data from Vermaat et al. (2000); *S. alterniflora* data from the measured velocity profile in the present study.

We here obtain a good fit ($p = 0.004$) between observed and predicted longitudinal dispersion before the dye slugs have fully mixed over depth. Therefore, our model appears to capture the necessary physics, and Eq. 12 may be used to estimate the final Fickian depth-shear dispersion constant. The Fickian limit is reached at $x_{Fickian} \approx 0.4h^2U/D_z$, or approximately $x_{Fickian} \approx 0.4(ud/D_z)h^2/d$. Taking $D_z/ud = 0.17$ and $d = 0.15$ cm based on observations, in a water depth of $h = 20$ cm, a slug is expected to mix fully across depth at a distance downstream of $x_{Fickian} \approx 60$ m. Because Fig. 7 indicates that stem-shear dispersion can be neglected at distances of >80 cm, based on our measured velocity profile and Eq. 12, we estimate that the normalized depth-shear dispersion constant $K_x/Uh \approx K_h/Uh \approx 9$. For $U = 3$ cm s^{-1}, this indicates that $K_x \approx K_h \approx 540$ cm^2 s^{-1}. For comparison, Chendorain et al. (1998) obtained a value of $K_x/Uh = 50$ in a study of longitudinal dispersion in a 46-cm–deep, 70-m–long emergent *Scirpus californicus* and *Scirpus acutus* wetland; *Scirpus* reeds have a similar, though not identical, morphology to *Spartina* species.

Discussion

The method used here to predict the velocity profile from morphology in a *S. alterniflora* canopy can be applied to other emergent salt marsh canopies (Fig. 9). The frontal area density profiles $a(z)$ from the present study and from two other *S. alterniflora* canopies (Burke and Stolzenbach 1983; Leonard and Luther 1995) and one *S. maritima* canopy (Neumeier and Ciavola 2004) are shown in Fig. 9A–D. These profiles and Eq. 3 are then used to calculate normalized velocity profiles $u(z)/\tilde{u}$, which are compared to measured velocity profiles in Fig. 9E–H. For these canopies there is good agreement between the measured and predicted velocity profiles, indicating that this method is a successful tool for velocity profile prediction. Figure 9 also shows that the shape of the $a(z)$ curve in the present study agrees well with *S. alterniflora* canopies elsewhere (Burke and Stolzenbach 1983; Leonard and Luther 1995) and also with a *S. maritima* canopy, which has a similar morphology to *S. alterniflora* (Neumeier and Ciavola 2004). Because a given plant species will tend to have a signature $a(z)/\tilde{a}$ curve, it is possible to estimate the $a(z)$ curve for a particular canopy given data on the stem density (which would determine the maximum value of a) and the total plant height (which would scale the profile with z).

Table 1. Predicted normalized depth-shear dispersion K_h/Uh for various species downstream of the distance $x_{Fickian}$ by which a cloud of particles has mixed over depth. Calculations assume $D_z/ud = 0.17$ and $d = 0.15$ cm. Dispersion predictions also use Eq. 12 and are based on the velocity profiles shown in Fig. 10.

Water depth, h (cm)	Distance to mix over depth, $x_{Fickian}$ (m)	Predicted normalized depth-shear dispersion, K_h/Uh		
		Atriplex portuloides	*Alisma gramineum*	*Spartina alterniflora*
20	60	0.8	17	9
40	250	—	24	40
60	550	—	30	60

We will now explore differences in dispersion due to differences in canopy morphology. Except for very close to the source, $K_h >> K_d$, so we will concentrate on understanding trends in K_h. The nondimensional shape function $\Im$ used to calculate the depth-shear dispersion can be calculated from the velocity profile $u(z)/\tilde{u}$ (Eq. 10). Figure 10 shows normalized vertical velocity profiles measured in several different species, along with a sketch showing each morphology (Vermaat et al. 2000; Leonard and Reed 2002). We here assume that the velocity approaches zero near the bed, even though measurements were not reported in this region. Table 1 shows estimates of the distance downstream by which a substance has mixed over depth, $x_{Fickian}$. These estimates reveal that in deeper water, a longer distance is necessary to mix over depth; at these larger length scales, other dispersive processes may become important. Table 1 also tabulates the corresponding normalized depth-shear dispersion constants K_h/Uh, assuming that the slugs have fully mixed over depth. Note that u must have a non-zero value at the bed for U/u to remain finite in Eq. 10; this integral is relatively insensitive to the exact value chosen. Because $K_h/Uh = f(h)$, the predicted depth-shear dispersion is shown for each species for a few different water depths. The different morphologies clearly produce different levels of dispersion: *Atriplex portuloides*, which has fairly uniform frontal area over depth, has a fairly constant velocity profile and generates a relatively low amount of depth-shear dispersion; *Alisma gramineum* exhibits more variation in frontal area and therefore produces more shear dispersion, but not as much as *S. alterniflora*. Finally, assuming that the bed shear velocity $u^* = 0.05$–$0.2\ U$, the classic open-channel dispersion equation $K_h = 5.9u^*h$ (Fischer et al. 1979, p. 125) would predict that $K_h/Uh = 0.3$–1, which is an order of magnitude smaller than what would be observed in an *Alisma gramineum* or *S. alterniflora* canopy if the Fickian limit is reached in both cases.

The above results show that, despite the complexities inherent in a field setting, it is possible to predict the shape of the longitudinal velocity profile and the longitudinal disper-

sion constant in an emergent aquatic canopy simply from knowledge of vegetation characteristics. Our analytic theory lumps all canopy complexity into the parameter a and assumes that $C_d = f(\mathrm{Re}_d)$ only. This theory can accommodate noncylindrical canopy elements if the drag coefficient $C_d(z)$ and frontal area $a(z)$ of the obstructions are known. For example, a flat-plate approximation for C_d may be more appropriate for a species with flat leaves, and the drag coefficient may need to be modified if stems are highly branched or clustered together (Gambi et al. 1990; Harvey et al. 1995; Wei and Chang 2002). This model also assumes that the frontal area $a(z)$ does not depend on $u(z)$, which is generally true for salt marsh plants but may not apply to all emergent canopies.

The above method of predicting the longitudinal dispersion constant is a powerful tool to parameterize the contribution of the stem- and depth-scale velocity heterogeneity to dispersion. Using this method, it is possible to predict the vertical velocity profile for many different emergent species with different morphologies, which will give rise to differing amounts of longitudinal depth-shear dispersion.

References

ACKERMAN, J. D. 2002. Diffusivity in a marine macrophyte canopy: Implications for submarine pollination and dispersal. Am. J. Bot **89:** 1119–1127.

AREGA, F., AND B. F. SANDERS. 2004. Dispersion model for tidal wetlands. J. Hydraul. Eng. **130:** 739–754.

BRAMPTON, A. H. 1992. Engineering significance of British saltmarshes, p. 115–122. *In* J. R. L. Allen and K. Pye [eds.], Saltmarshes: Morphodynamics, conservation, and engineering significance. Cambridge Univ. Press.

BURKE, R. W., AND K. D. STOLZENBACH. 1983. Free surface flow through salt marsh grass. Tech. Rep. MITSG 83-16, Massachusetts Institute of Technology.

CHENDORAIN, M., M. YATES, AND F. VILLEGAS. 1998. The fate and transport of viruses through surface water constructed wetlands. J. Environ. Qual. **27:** 1451–1458.

CHERBLANC, F., A. AHMADI, AND M. QUINTARD. 2003. Two-medium description of dispersion in heterogeneous porous media: Calculation of macroscopic properties. Water Resources Res. **39:** doi:10.1029/2002WR001559.

CHRISTIANSEN, T., P. L. WIBERG, AND T. G. MILLIGAN. 2000. Flow and sediment transport on a tidal salt marsh surface. Estuar. Coastal Shelf Sci. **50:** 315–331.

FINELLI, C. M. 2000. Velocity and concentration distributions in turbulent odor plumes in the presence of vegetation mimics: A flume study. Mar. Ecol. Prog. Ser. **207:** 297–309.

———, D. D. HART, AND R. A. MERZ. 2002. Stream insects as passive suspension feeders: Effects of velocity and food concentration on feeding performance. Oecologia **131:** 145–153.

FISCHER, H. B., E. J. LIST, R. C. Y. KOH, J. IMBERGER, AND N. H. BROOKS. 1979. Mixing in inland and coastal waters. Academic.

FONSECA, D. M., AND D. D. HART. 1996. Density-dependent dispersal of black fly neonates is mediated by flow. Oikos **75:** 49–58.

GAMBI, M. C., A. R. M. NOWELL, AND P. A. JUMARS. 1990. Flume observations on flow dynamics in *Zostera marina* (eelgrass) beds. Mar. Ecol. Prog. Ser. **61:** 159–169.

HARVEY, M., E. BOURGET, AND R. G. INGRAM. 1995. Experimental evidence of passive accumulation of marine bivalve larvae on filamentous epibenthic structures. Limnol. Oceanogr. **40:** 94–104.

HOSOKAWA, Y., AND T. HORIE. 1992. Flow and particulate nutrient removal by wetland with emergent macrophyte, p. 1271–1282. *In* R. Vollenweider, R. Marchetti, and R. Vivani [eds.]. Marine Coastal Eutrophication. Elsevier. Sci. Total Environ. (suppl.) 1271–1282.

JENTER, H. L., AND M. P. DUFF. 1999. Locally-forced wind effects on shallow waters with emergent vegetation. *In* Proc. Third Int. Symp. Ecohydraulics. IAHR.

KOCH, D. L., AND A. J. C. LADD. 1997. Moderate Reynolds number flows through periodic and random arrays of aligned cylinders. J. Fluid Mech. **349:** 31–66.

KOCH, E. W. 1994. Hydrodynamics, diffusion-boundary layers and photosynthesis of the seagrasses *Thaliassia testudinum* and *Cymodocea nodosa*. Mar. Biol. **118:** 767–776.

———, AND M. HUETTEL. 2000. The impact of single seagrass shoots on solute fluxes between the water column and permeable sediments. Biol. Mar. Medit. **7:** 235–239.

LEONARD, L. A., AND M. E. LUTHER. 1995. Flow hydrodynamics in tidal marsh canopies. Limnol. Oceanogr. **40:** 1474–1484.

———, AND D. J. REED. 2002. Hydrodynamics and sediment transport through tidal marsh canopies. J. Coastal Res. **SI36:** 459–469.

LÓPEZ, F., AND M. GARCÍA. 1998. Open-channel flow through simulated vegetation: Suspended sediment transport modeling. Water Resources Res. **34:** 2341–2352.

MAURI, R., AND S. HABER. 1986. Applications of Wiener's path integral for the diffusion of Brownian particles in shear flows. SIAM J. Appl. Math. **46:** 49–55.

MIDDLETON, B. 2000. Hydrochory, seed banks, and regeneration dynamics along the landscape boundaries of a forested wetland. Plant Ecol. **146:** 169–184.

MITSCH, W. J., AND J. G. GOSSELINK. 1986. Wetlands. Van Nostrand Reinhold.

NEARY, V. S. 2003. Numerical solution of fully developed flow with vegetative resistance. J. Eng. Mech. **129:** 558–563.

NEPF, H. M. 1999. Drag, turbulence, and diffusion in flow through emergent vegetation. Water Resources Res. **35:** 479–489.

———. 2004. Vegetated flow dynamics, p. 137–164. *In* S. Fagherazzi, M. Marani, and L. Blum [eds.], Ecogeomorphology of tidal marshes. Coastal Estuar. Monogr. Ser. **59:** doi:10.1029/59CE09.

———, J. A. SULLIVAN, AND R. A. ZAVISTOSKI. 1997. A model for diffusion within emergent vegetation. Limnol. Oceanogr. **42:** 1735–1745.

NEUMEIER, U., AND P. CIAVOLA. 2004. Flow resistance and associated sedimentary processes in a *Spartina maritima* salt-marsh. J. Coastal Res. **20:** 435–447.

PETERSON, C. G. 1996. Mechanisms of lotic microalgal colonization following space-clearing disturbances acting at different spatial scales. Oikos **77:** 417–435.

PETERSON, C. H., R. A. LUETTICH, JR., F. MICHELI, AND G. A. SKILLETER. 2004. Attenuation of water flow inside seagrass canopies of differing structure. Mar. Ecol. Prog. Ser. **268:** 81–92.

PROFFITT, C. R., S. E. TRAVIS, AND K. R. EDWARDS. 2003. Genotype and elevation influence *Spartina alterniflora* colonization and growth in a created salt marsh. Ecol. Appl. **13:** 180–192.

RINALDO, A., A. MARANI, AND R. RIGON. 1991. Geomorphological dispersion. Water Resources Res. **27:** 513–525.

RUSSO, D. 2003. Simulation of transport in three-dimensional heterogeneous unsaturated soils with upscaled dispersion coefficients. Water Resources Res. **39:** doi:10.1029/2003WR002245.

SAIERS, J. E., J. W. HARVEY, AND S. E. MYLON. 2003. Surface-water transport of suspended matter through wetland vegeta-

tion of the Florida everglades. Geophys. Res. Lett. **30:** doi: 10.1029/2003GL018132.

SHI, Z., J. S. PETHICK, AND K. PYE. 1995. Flow structure in and above the various heights of a saltmarsh canopy: A laboratory flume study. J. Coastal Res. **11:** 1204–1209.

SILBERHORN, G. M. 1982. Common plants of the Mid-Atlantic coast. Johns Hopkins Univ. Press.

SMITH, R., AND N. C. DAISH. 1991. Dispersion far downstream of a river junction. Phys. Fluids A **3:** 1102–1109.

STONE, B. M., AND H. T. SHEN. 2002. Hydraulic resistance of flow in channels with cylindrical roughness. J. Hydraul. Eng. **128:** 500–506.

THOMPSON, J. R., H. REFSTRUP SØRENSON, H. GAVIN, AND A. REFSGAARD. 2004. Application of the coupled MIKE SHE/MIKE 11 modelling system to a lowland wet grassland in southeast England. J. Hydrol. **293:** 151–179; doi:10.1016/j.jhydrol. 2004.01.017.

VALIELA, I., J. M. TEAL, AND W. G. DEUSER. 1978. The nature of growth forms in the salt marsh grass *Spartina alterniflora*. Am. Nat. **112:** 461–470.

VERMAAT, J. E., L. SANTAMARIA, AND P. J. ROOS. 2000. Water flow across and sediment trapping in submerged macrophyte beds of contrasting growth form. Arch. Hydrobiol. **148:** 549–562.

WEI, C. Y., AND J. R. CHANG. 2002. Wake and base-bleed flow downstream of bluff bodies with different geometry. Exp. Therm. Fluid Sci. **26:** 39–52.

WHITE, B. L., AND H. M. NEPF. 2003. Scalar transport in random cylinder arrays at moderate Reynolds number. J. Fluid Mech. **487:** 43–79.

WHITE, F. M. 1991. Viscous fluid flow. McGraw-Hill.

Received: 12 April 2005
Accepted: 28 July 2005
Amended: 9 September 2005